SPE
Society of Petroleum Engineers

SPE 17598

How Successful Acid-Frac Program Could Require Drastic Changes in Both Drilling and Completion Design

by D. Despax, and C. Bladier and P. Charlez, Total-CFP

SPE Members

This paper was prepared for presentation at the SPE International Meeting on Petroleum Engineering, held in Tianjin, China, November 1–4, 1988.

INTRODUCTION AND HISTORICAL BACKGROUND

This article is based on five years experience in acid fracturing on a Middle East offshore field operated by TOTAL-CFP.

The field in question is a highly stratified formation containing dolomitic reservoirs which are separated by very compact and almost impermeable anhydritic interbeds. [FIG. 1]

The producing layers (A, B, C, D and E) vary in thickness and two of these are of particular interest: «A», which has already been considerably depleted with a fairly high matrix permeability (150 to 200 mD) and «E» only slightly depleted, and with a much lower matrix permeability (25 to 30 mD).

The main question was the following :

- What would be the best theoretical acid frac we could implement in layer «E» (and what resulting medium-term gain in production could be expected) allowing for the major constraint that communication must not be created between E and A, as the latter is much more permeable and had a very high water cut when producing previously ?

The first five jobs were carried out between 1981 and 1984, pumping acid through a 7", cemented and perforated liner. Only one of these treatments can be considered successful, as it was the only one to provide adequate containment.

For the other jobs, production gains were negligable, due to the fact that only a small part of the acid volume penetrated the selected layer (E) whereas most of the treatment leaked upwards, probably mostly into level A, considerably increasing the watercut in the well.

Following these disappointing results, an in depth-investigation was run, with three parts :

- a containment study,
- study on the liner cement strength,
- optimization of the treatment.

1. STATUS OF THE PROBLEM

The mechanical problem of containment can be understood by applying a simple analogy which reveals parameters of the first importance.

The analogy [FIG. 2] is that of a rigid table on which we put a flexible metal sheet with a small tube through the middle and heavy stones placed on the edges. If fluid is injected via the tube, between the table and the metal sheet, it will tend to flow perpendicular to the sheet (direction z), as this will require less energy than is needed to lift the stones. However, when the fluid reaches a great distance from the injection point, the pressure loss in direction z, may become preponderant and the fluid, which will always seek the solution demanding the least energy, will lift the stones.

This simple analogy shows that the problem of containment is merely a problem relating to energy, and that the difference in minor principle stresses between the reservoir and interbeds (the weight of the stones in the analogy) plays a fundamental role.

Two other parameters are of primary importance, first the Young modulus of the various levels (the analogy is that of a metal sheet with a variable thickness placed on the table and second the surface energy of these levels (different adhesion of the sheet to the table).

In short, three categories of mechanical parameters will play a deciding role in containment : the stresses, the moduli and surface energies. In addition the fluid loss coefficients of the various levels, plus the viscosity of the fracturing fluid, will all have an indirect influence.

OILCRACK is a 3D finite element code, which simulates the propagation of a vertical fracture in a horizontally stratified formation whose layers can have different stresses, elastic moduli and surface energies.

A complete study has been undertaken to attempt to quantify the quality of the containment on the field concerned.

2 DETERMINATION OF EXPERIMENTAL PARAMETERS IN THE LABORATORY

First of all, three kinds of test were carried out in the laboratory : standard measurements of the elastic modulus in a triaxial cell, then surface energy measurements (by bending tests at three points [FIG. 3]) and finally stress measurements using the differential Strain Curve Analysis (DSCA). Tests were run on cores from two different wells : A27 and A28. The results of the modulus and surface energy measurements are given below :

		E (bar) x 10^{-3}		2 (J/m^2)
A	reservoir	242	.16	5
E_1	interbed	398	.03	7.8
B	reservoir	205	.12	8
E_2	interbed	385	.04	35.2
C	reservoir	300	.10	·
E_3	interbed	475	.06	8.5
D	reservoir	330	.12	·
E_4	interbed	398	.07	·
E	reservoir	220	.13	5.2

TABLE 1

RESULTS OF MODULUS AND SURFACE ENERGY MEASUREMENTS

As can be seen, the results show that the interbeds are stiffer than the reservoirs but that this difference is not so great as the difference in porosity would indicate (15 % for the reservoirs and several per thousands for the anhydritic interbeds).

The surface energies are also fairly homogeneous (except for interbed E_2 between the reservoirs B and C).

Stresses were measured using the original DSCA method. Below, we recall the basic theory of this method. For further details see Charlez Ph, Hamamdjian C and Despax D [1986].

This interpretation method is based on the fact that any rock sample taken from within the formation will retain, in its matrix, a memory of the effective stress it underwent «in situ». This memory can be seen particularly in the intensity of the microfissuring. In effect, when a sample is taken (by coring for instance), the material is freed from the initial state, and, following this release, microcracks will appear in proportion to the preexisting state of stress.

An oriented cube-shaped sample (orientation is possible only where the well is not perpendicular to the stratification) is then cut and replaced, in the laboratory, under hydrostatic pressure inside a special cell. Resistive deformation gauges [FIG. 4] fixed to the sides will record the deformation stress curves. These will be as shown in FIG. 5 : under an increasing pressure, P, a first phase (OA) will be observed in which the microcracks close gradually, then the material will adopt a linear elastic behaviour (AB). At any point on the curve, the total deformation is therefore equal to the sum of the two elementary deformations. One, ϵ_{ij}^{f}, is due solely to the closing of the microfissures, and the other, to the elasticity of the material. The deformations measured in 9 directions, six of which are independent (1 = 4, 3 = 9, 6 = 7), make it possible to determine the tensor $\underset{\sim}{\epsilon f}$. According to the hypothesis formulated :

$$\underset{\sim}{\sigma^*} = \lambda \, \underset{\sim}{\epsilon f}$$

The coefficient of proportionality λ can be calculated assuming that the absolute vertical stress is equal the overburden (no vertical tectonic stress), i.e. :

$$\sigma^*_{zz} = \rho_m \, gz - \alpha \, P_R$$

where ρ_m is the average specific gravity of the overburden , z the depth, P_R the reservoir pressure, and α the Biot coefficient.

The tests were performed on 37 samples from two different wells and give specially good results for the reservoirs (porous, therefore data-bearing), rather poor results for the interbeds (stiffer with very low porosity). However, as yet the method is not reliable enough to give a value of stress per layer, but rather an average for all the levels together, summarized in the table below :

WELL	z (m)	σ_3 (bar)	σ_1 (bar)	σ_2 (bar)	θ (°)	φ (°)
A	2313	417	484	572	E 69°S	81
B	2343	418	549	608	E 55°S	89
A + B	2328	421	529	581	E 59°S	85

TABLE 2
RESULTS OF DSCA
(θ IS THE AZIMUTH AND φ THE INCLINATION OF σ_1)

It should be noted that orientations obtained for the stresses show a subvertical major principle stress, σ_2 and subhorizontal intermediate and minor stresses. Replaced in the geographical context, these show the direction of the major horizontal components to be perpendicular to the axis of the Gulf, which corresponds well with the local tectonics [FIG. 6].

3. NUMERICAL SIMULATIONS OF CONTAINMENT PARAMETRIC STUDY

a/ Fracturing of the E reservoir only

A first simulation has been performed with a 3 layer geometry : reservoir E and its two anhydritic barriers. The parameters used for this 3 layers problem are summarized in table 3 :

LAYER	h (m)	E(10^{10} Pa)	ν	2γ (J/m2)	DENOMINATION
1	9	3.4	0.1	20	barrier
2	7	2.5	0.1	10	reservoir E
3	11	4.0	0.1	22	barrier

TABLE 3

IDENTIFICATION

In this table, h is the thickness of the layer, E, ν, and 2γ its elsatic modulus, Poisson's ratio and surface energy respectively.

The fluid viscosity has been taken as 0.8 Cp. In a first hypothesis it was assumed that the fracture prevents initiation into the barrier (infinite in situ stress or infinite surface energy 2γ in the barriers). The results of these computations led to the following conclusions :

- The fluid loss coefficient C_w is a dominating factor, the injection pressure and the fracture length strongly depending on the C_w [FIGS. 7 AND 8], the pressure and length increase faster as the C_w decreases. However, in the two cases presented on fig. 7, it can be seen that the perfect containment of the fracture demands a very high pressure (up to σ_3) which can reach 90 bar in the case of a small C_w. In a second case (still with the same geometry and the same mechanical properties), barrier penetration is provided by adding two more degrees of freedom λ_1 and λ_2 to the previous rectangular crack [FIG. 9] and simulating penetration height and length. An excess of stress $\Delta\sigma$ is imposed in the interbeds. Two computations were carried out and show that :

  1/ With 60 bars of barrier stress, the crack does not remain contained. Although after 71.32 seconds, the fracture is only 234 meters long, a penetration of 345 cm was computed.

  2/ The effectiveness of the barrier stress increases rapidly. With a 100 bar stress, the initiation was to 225 cm at the crack entrance after 942 seconds, and to 265 cm after 1508 seconds, meaning that the barrier holds.

Compared to runs with imposed containment, we observe a drop in the well pressure of 25 to 30 %. The maximum fracture width is approximately 10 % less. However, the pressure remains considerably greater than the minimal in situ stress σ_3, which would not be the case in a classical 2D model.

b/ Fracturing of reservoirs b, c, d together

In the second phase of the study, we took the case of three adjacent reservoirs, B, C and D, to be fractured simultaneously. It is estimated that the internal barriers, between B and C and between C and D are fractured along with the reservoirs. In practice, this part of the crack was modelled by a single vertical front, crossing all five layers. As in the first simulation, the barrier between, D and E which is now the lower barrier, is critical, because its elasticity and in situ stress are the same as in the upper barrier, while the latter is twice as thick. The fracturing fluid was specified as follows :

- Fluid leak-off coefficient $C_W = 0\ m/\sqrt{s}$ (no losses)
- Injected volume $V_t = 90\ m^3$ (two crack wings)
- Injection rated $Q = 1.6\ m^3/min$ (two crack wings)

With these considerations, the case again reduces to a three-layer problem. For the generalized reservoir, i.e. the five layers described above, the toughness of the internal barriers was taken into account by computing an equivalent, global surface energy and an equivalent elastic modulus. Table 4 shows the final set of data :

LAYER	h (m)	E(10^{10} Pa)	ν	2γ (J/m2)	DENOMINATION
1	6	4.0	0.1	30	barrier
2	13	2.9	0.1	13	reservoir
3	3	4.0	0.1	20	barrier

TABLE 4

SET OF PARAMETERS FOR COMPUTATIONS

Two types of simulations were performed with this type of geometry.

At first we used a non newtonian fluid with high viscosity (200 Cpoise) and a zero fluid loss coefficient. Several runs were realised for the first one, restricted to the reservoir, the well pressure [FIG. 10] reached very high values (111.5 bar for 3315 seconds of injection) for a final length of 852 m. On the other hand several single-step runs were done with varying barrier stresses (60 bar - 100 bar - 125 bar - 150 bar). While the first three values proved to be largely insufficient, the 150 bar stress corresponds to a penetration of over 304 cm, which is only slightly more than the barrier thickness. Hence, the barrier stress necessary for containment must be estimated slighty over 150 bar. Furthermore OILCRACK-3D computed a total crack length of 858 meters in the reservoir and 785 m at the barrier interface. The crack widths at the well were 0.99 cm at the center, 0.27 cm at the barrier interface and 0.93 cm halfway between. The entrance pressure was 82.9 bar (as compared to 111.5 bar without barrier penetration).

The last case is similar to the previous one (B-C-D fracturation) but this time we used a low viscosity newtonian fluid , (0.5 Cp) a non zero C_w (0.008 cm/$\sqrt{s}$) and a 50 bar difference. In this case, barrier penetration is only 49.9 cm (compared with 3 m in the previous case with 150 bar of $\Delta\sigma$), and well pressure is much lower (23 bar).

All the results of the similations lead to the following conclusions :

- OILCRACK-3D apparently produces realistic calculations.
- OILCRACK-3D clearly identified three-dimensional effects : pressures are much higher than expected from 2-D estimations.
- Confining in situ stresses are very important and represent the main factor to stop barrier detrioration by crack penetration. 100 to 150 bar at least is necessary to stop barrier penetration.
- Fluid viscosity is an important parameter since it has a tendency to yield higher pressures at the fracture entrance and to cause barrier rupture.
- Another essential parameter is the fluid leak-off rate. High fluid loss coefficient releases pressure.

One more parameter has been taken into account : the injection flow rate. Several flow rates were tested for fracturing level E only. The results show that the wellbore pressure always increases with time but is lower if the flow rate decreases [FIG. 11].

In situ stress measurements

This parametric study having clearly showed the primary importance of the minimal principal stress on containment, it was decided to perform a minifrac program in the reservoir E and in the interbed D-E to evaluate stresses in these levels.

The first stress test on level E showed a stress equal to 300 bar ± 10 bar [FIG. 12] and the value obtained in the interbed was 580 bar ± 10 bar.

The value obtained by the stress test in level E (300 bar) was very different from that evaluated by DSA (417 bar - Table 2). This can be explained by the different locations of the two wells on which these measurements were realized (the well on which the DSA was realized lies inside a faulted zone) and by the fact that the values obtained by DSA is an average state of stress for the different layers.

Compared with the results of 3D numerical simulations, we can conclude from these values that the source of communication lies in channelling of the acid through the cement annulus and not via the interbeds, which provide good containment.

5. BEHAVIOUR OF THE CEMENT DURING THE TREATMENT

It was possible to analyse the stress distribution in the cement annulus using a finite element, 3D model. This model showed clearly [FIG. 13] that there was a discontinuity in the principle minor stress when passing from the cement to the formation, and that this discontinuity depended considerably on the ratio between the Young's modulus of the rock and that of the cement. In brief it can be said that the greater the elastic modulus of the cement compared to that of the rok, the greater the traction stress to which the cement will be subjected [FIG. 13]. The traction strength of the cement usually being lower than that of the rock, the risk of the cement yielding will be high. The poor containment of the fracture can therefore easily be explained by a poor mechanical strength of the cement.

6. DESIGN OF THE TREATMENT

The design of the treatment and the prediction of post-fracturing production (i.e. fracture conductivity) has been computed by the 2D simulator OILFRAC. This program takes into account the following basic phenomena :

- rock elasticity,
- fluids flow and rheologies,
- chemical reactions,
- thermal transfers.

Three basic hypothesis have been considered when writing this program :

- Reservoir or layer concerned is homogeneous, isotropic, elastic and of constant thickness, perpendicular to the minimum component of the stress tensor.
- Fracture is oriented vertically across the well.
- Rock is only deformed horizontally, leading to a two- dimensional simulation.
- The fluid rheology is a power law k', n'.

OILFRAC simulates the fracture propagation over some distance by constant length steps, and this for a given reservoir, a given set of fluids characteristics, a given set of injection rates.

At the end of each length step fractured, the computer provides the following profiles versus fracture length reached :

- width profile,
- temperature profile,
- pressure profile,
- width etched by acid,
- acid concentration profile,
- fluid rate profiles.

INPUT DATA has been provided by laboratory direct measurement described above.

The following parameters used in the OILFRAC program were :

- reservoir temperature (measured on site) : 90°C,
- YOUNG's modulus (derived from lab experiments) : 1.72 10^{10} Pa (average) ;
- POISSON's ratio (derived from lab experiments) : 0.2,
- tenacity fixed by user : 3 to 9 10^{5} Pa√m
- specific rock factor : 1 for limestone, 0.66 for dolomite,
- porosity from reservoir data : 14 %,
- rock solubility : 97 %
- horizontal stress derived from stress measurement by DSCA : 417 bar ;
- reservoir height (reservoir data) : 7 m,
- number of fluids injected : 1 (acid HCl 7,5 x up to 32 x) and 2 (viscous pad followed by HCl) ;
- fracturing steps of 25 to 100 m,
- fluid loss coefficient from 8 10^{-5} to 40 10^{-5} m/√s ;

Firstly two sets of simulations were run to evaluate the sensitivity of the model to acid injection rate and fluid loss coefficient C_w.

At low rates (10 BPM), the acid reaction rate increases near the wellbore due to high temperature [FIG. 14]. A shorter penetration distance is then observed.

At high rates (50 BPM), thermal exchange with rock is reduced leading to greater penetration distances.

It should be noticed that if we assume a 1 mm cut off on the etched width, a greater volume of acid is necessary at 50 BPM than at 25 BPM, but fracture length will be greater in that case.

The fracture geometry is also considerably controlled by the rate of acid fluid loss through the fracture walls [FIG. 15].

For a typical reservoir like E (30 mD), we can expect high fluid losses, due to relatively high permeabilities and high differential pressure at the well bore.

Minifrac shut in with water base mud, gave a value of 7.3 10^{-5} m/√s.

In a final more realistic simulation, we assume an acid-boat available with an initial volume of 32 x chlorhydric acid (64000 gallons).

Three water dilutions were considered : 28 x, 15 x, 7.5 x. [FIG. 16, 17, 18]

A high injection rate of 50 BPM, and a fluid loss coefficient of 31 10^{-5} m/√s were chosen.

Perfect drainage criterion

A perfect drainage of the fracture is obtained when the ratio of conductivities (fracture/formation) is at least greater than 10.

$$KW / kL > 10$$

where :

K is the equivalent permeability of the fracture (mD)

k is the formation permeability (mD)

L is the length of the fracture

w is the fracture etched width.

Theory shows that permeability of the acid fracture can be derived from a two-plane system fluid flow.

$K = w^2 / 12$ w : distance between the two planes

Therefore fracture conductivity will be Kw or $w^3/12$.

When applied to the perfect drainage criteria, a relation between w and L is derived.

$$w > (12 \times k \times L)^{1/3} \times (10)^{1/3}$$

In our case (k = 30 mD), according to the ratio of the criterion above, we obtain according to limit-of-conductivities ratio :

ratio > 10 $w > L^{1/3} \times 15.3\ 10^{-5}$

ratio > 100 $w > L^{1/3} \times 33.0\ 10^{-5}$

ratio > 300 $w > L^{1/4} \times 47.4\ 10^{-5}$

As an example, if we wish for a 300 m long fracture the etched width cut off should be : 1, 2.2 and 3.2 mm.

Looking at figure 17 (HCl 15 x), and considering a 2.2 mm etched width cut off, we note that a 300 m long fracture needs a volume of acid slightly over 112800 gallons, and that the maximum length will be 355 m if we inject up to 155400 gallons.

With different dilutions, the conductive fracture lengths will vary with cut off criteria.

CUTT OFF	HCl 28 x	HCl 15 x	HCl 7.5 x
1 mm	350 m	430 m	500 m
2 mm	205 m	370 m	430 m
2.3 mm	175 m	355 m	420 m

In fact, we have assumed the same fluid loss coefficient for the three fluids and as viscosities are different, some corrections should be made to the fracture lengths (7.5 x acid filter more than 28 x acid, leading to a smaller gap between fracture lengths).

We can conclude that with a cut-off value of 1 mm, a 400 m long fracture is feasible.

In cases where conductivity criteria are more conservative (cut off of 2 mm), a 300 m long fracture can be expected.

Evaluation of post treatment production

Post treatment theoretical production can be evaluated by a reservoir computation summarized on figure 18.

If we assume a perfect drain of dimensionless conductivity FD equal to 10^3, we can evaluate the dimensionless time tD for the first six months cumulative production.

$$t_D = \beta \frac{F_D^2 k^3 t}{\phi \mu Ct (KW)^2}$$

where all the parameters are described on figure 19. Taking into account that $KW = 10^3 kL$ where L is the length of the perfect drain, we obtain :

$$t_D = \frac{kt}{\phi \mu Ct L^2}$$

In our case :

$k = 30\ mD = 30\ 10^{-15}\ m^2$ $\quad t = 6\ months = 1.575\ 10^7\ s$

$\phi = 0.14$ $\quad L = 300\ m$

$\mu = 0.8\ Cp = 8\ 10^{-4}\ Pas$ $\quad B = 1.32$

$C_t = 2\ 10^{-5}\ psi^{-1} = 2.910^{-9}\ Pa^{-1}$

$$==> t_D = 16 \quad ==> \frac{t_D}{F_D^2} = 1.610^{-2}$$

The dimensionless mean flow rate is then [FIG. 19] $8\ 10^{-1}$. We can finally compute the cumulative oil theoretical production N for the first six months post treatment.

$$N = \frac{2\pi \frac{N_D}{t_D} k h \Delta p t}{B \mu}$$

where Δp is the pressure drop (41 bar)

$$N = 60.513\ m^3$$

corresponding to an average flowrate of 2155 BPD for level E during the first six months.

4. FINAL OPERATION AND CONCLUSIONS

The conclusions of these different studies suggest level E being fractured open hole, using and external casing packer to isolate level E from higher reservoirs. This procedure had its first success during 1987, the fracure remaining perfectly contained within reservoir E (as can be clearly seen on the thermometer log [FIG. 20]. However, this first open hole treatment was intentionally kept small volume (30000 gallons of HCl 15 %).

In conclusion, problems of poor containment seem therefore to come principally from the cementing quality. Further tests will certainly confirm this, and hence, open hole as a good final solution.

ACKNOWLEDGEMENTS

We thank TOTAL-CFP to allow the publication of this paper.

REFERENCES

1. Charlez Ph, Hamamdjian C. and Despax D. : «To the microcracking of a rock a memory of its initial state of stress ? » Proceedings of the International Symposium on Rock Stress and Rock Stress Measurements, Stockholm, 1-3 September (1986).

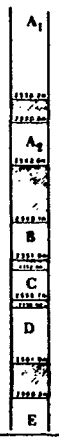

Fig. 1. Statigraphy of the field

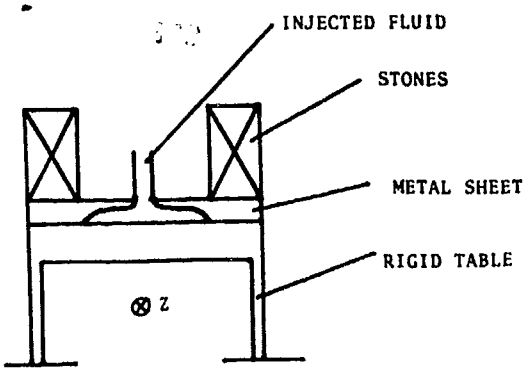

Fig. 2. Analogy of the containment problem

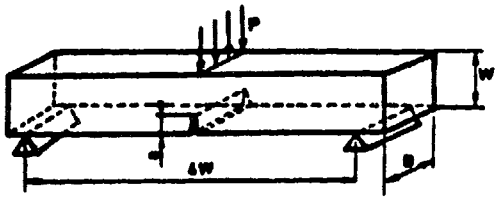

Fig. 3. Bending test to determine surface energy

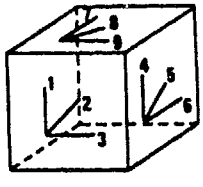

Fig. 4. DSCA : positionning of the gauges on the sample

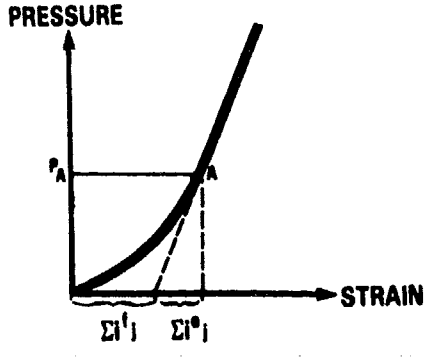

Fig. 5. DSCA : deformation stress curve

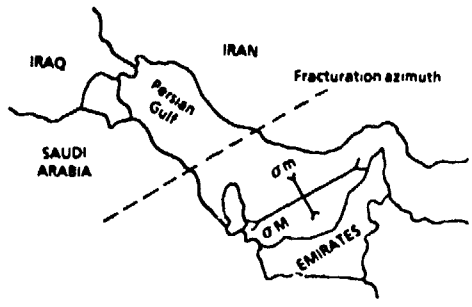

Fig. 6. Geographic orientation of the horizontal state of stress

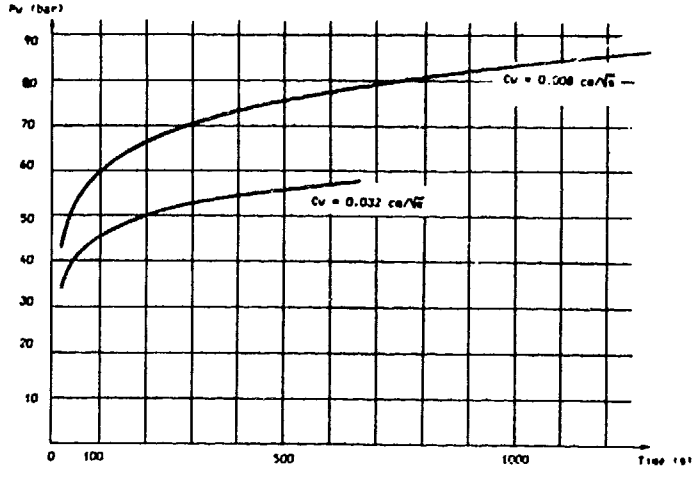

Fig. 7. Propagation restrained to E reservoir - Influence of C_W (pressure history)

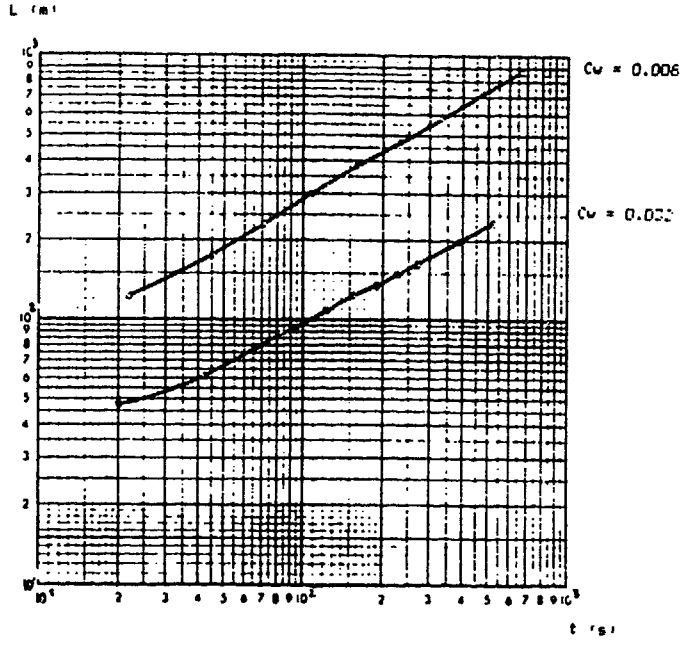

Fig. 8. Propagation restrained to E reservoir - Influence of C_W (length history)

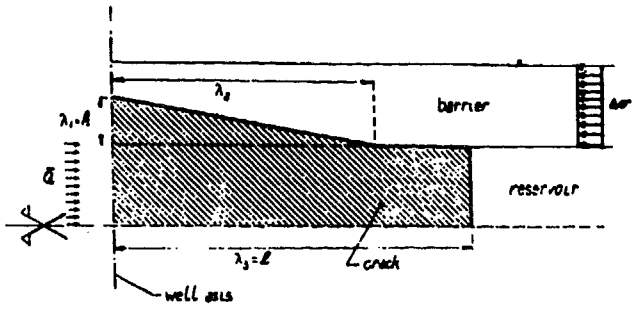

Fig. 9. Fracture geometry description when unconfined

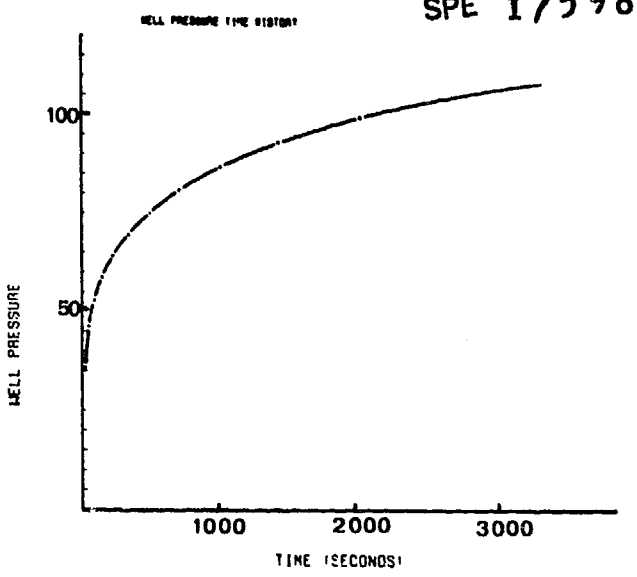

Fig. 10 Propagation restrained to B-C-D reservoirs with a 200 Cp viscosity.

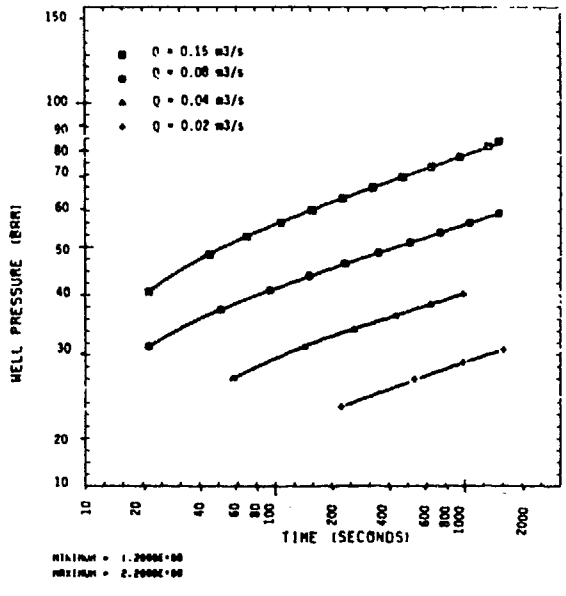

Fig. 11 Level E - Influence of flow rate on well pressure

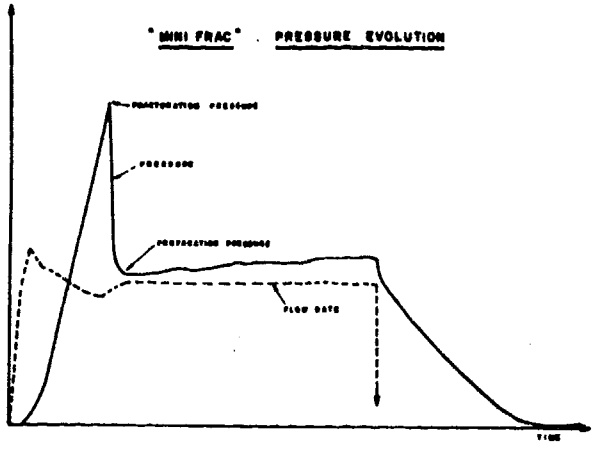

Fig. 12 Stress test in level E

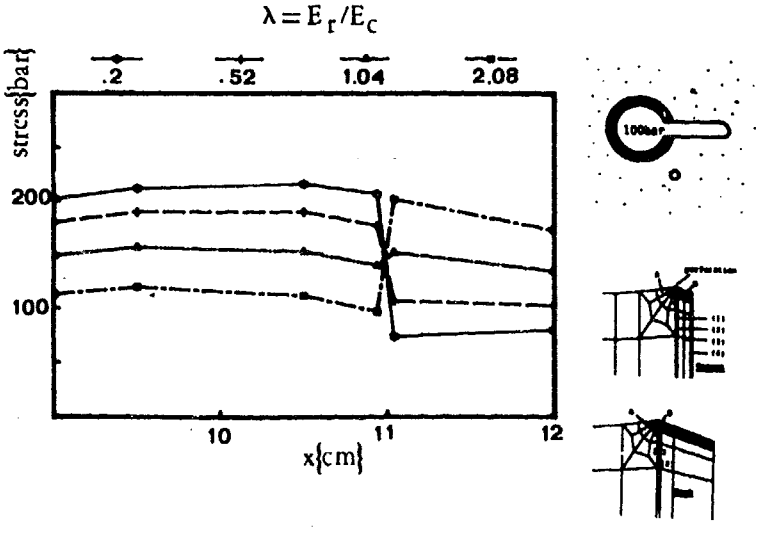

Fig. 13 Fracturing of a cement ring - Influence of the modulus ratio on the principle minor stress

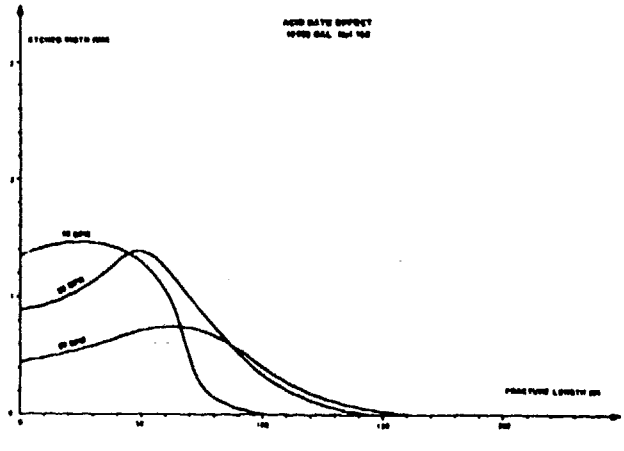

Fig. 14 Acid rate effect on fracture profile

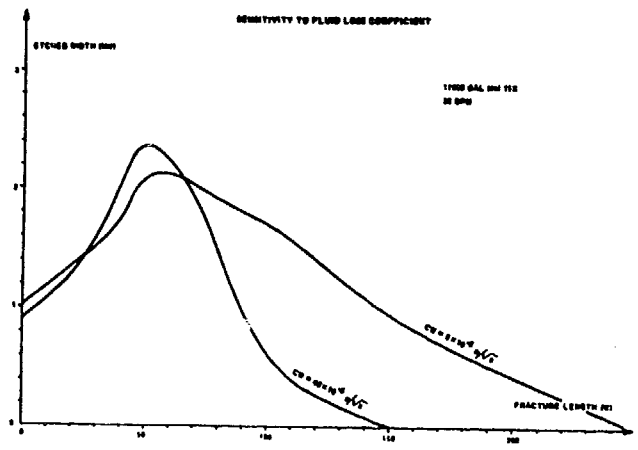

Fig. 15 Fluid loss coefficient effect on fracture profile

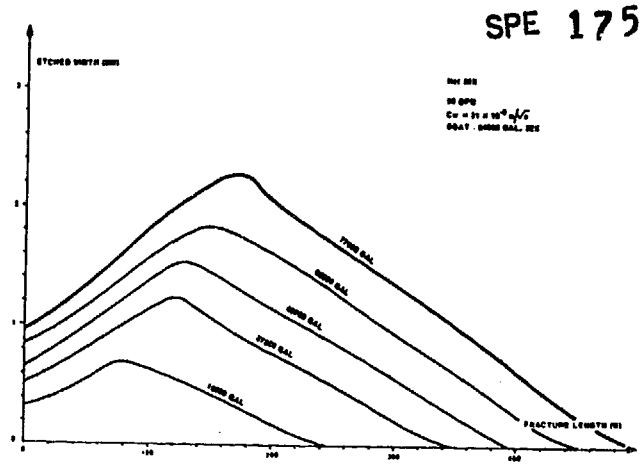

Fig. 16 Effect of acid dilution on fracture profile (28 x)

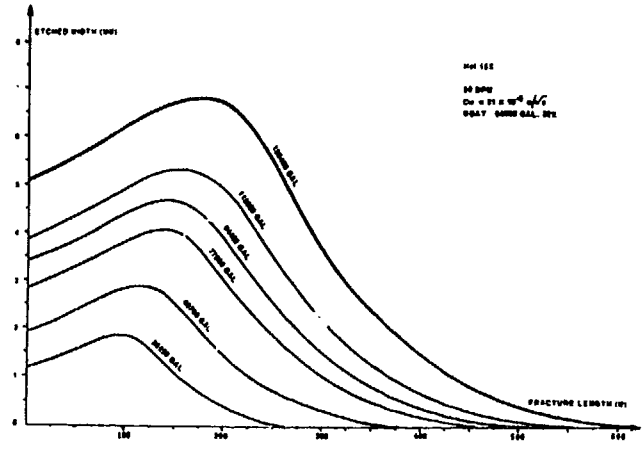

Fig. 17 Effect of acid dilution on fracture profile (15 x)

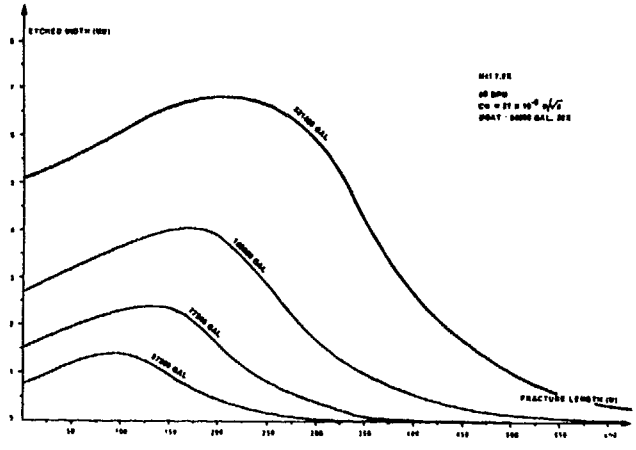

Fig. 18 Effect of acid dilution on fracture profile (7.5 x)

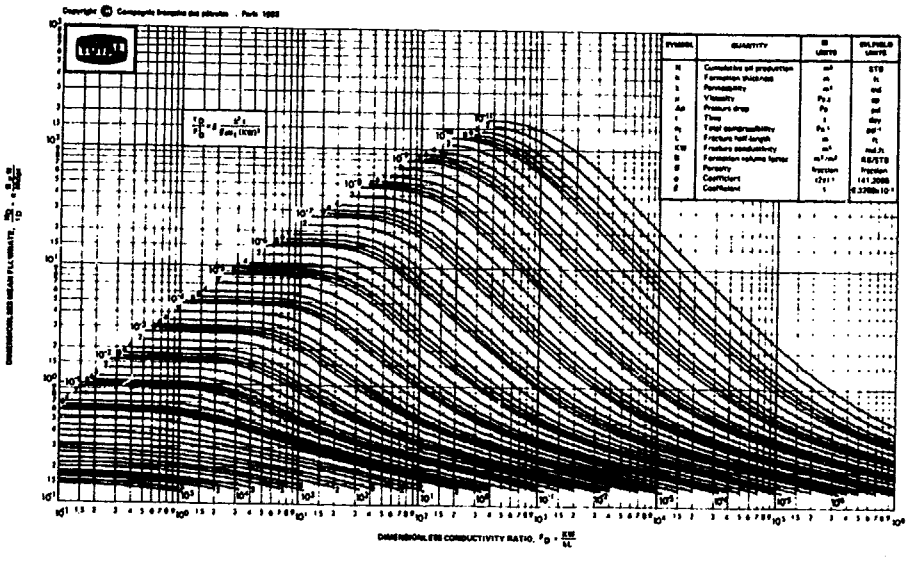

Fig. 19 Dimensionless mean flowrate of a fractured well in an infinite reservoir as a function of dimensionless conductivity ratio and dimensionless production time divided by dimensionless conductivity ratio squared

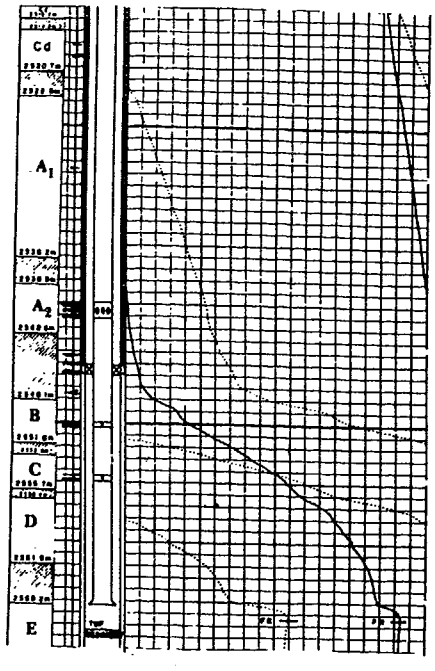

Fig. 20 Temperature log after frac in open hole